



UvA-DARE (Digital Academic Repository)

Mechanistic Basis for Red Light Switching of Azonium Ions

Medved', M.; Di Donato, M.; Buma, W.J.; Laurent, A.D.; Lameijer, L.; Hrivnák, T.; Romanov, I.; Tran, S.; Feringa, B.L.; Szymanski, W.; Woolley, G.A.

DOI

[10.1021/jacs.3c06157](https://doi.org/10.1021/jacs.3c06157)

Publication date

2023

Document Version

Final published version

Published in

Journal of the American Chemical Society

License

Article 25fa Dutch Copyright Act (<https://www.openaccess.nl/en/in-the-netherlands/you-share-we-take-care>)

[Link to publication](#)

Citation for published version (APA):

Medved', M., Di Donato, M., Buma, W. J., Laurent, A. D., Lameijer, L., Hrivnák, T., Romanov, I., Tran, S., Feringa, B. L., Szymanski, W., & Woolley, G. A. (2023). Mechanistic Basis for Red Light Switching of Azonium Ions. *Journal of the American Chemical Society*, 145(36), 19894-19902. <https://doi.org/10.1021/jacs.3c06157>

General rights

It is not permitted to download or to forward/distribute the text or part of it without the consent of the author(s) and/or copyright holder(s), other than for strictly personal, individual use, unless the work is under an open content license (like Creative Commons).

Disclaimer/Complaints regulations

If you believe that digital publication of certain material infringes any of your rights or (privacy) interests, please let the Library know, stating your reasons. In case of a legitimate complaint, the Library will make the material inaccessible and/or remove it from the website. Please Ask the Library: <https://uba.uva.nl/en/contact>, or a letter to: Library of the University of Amsterdam, Secretariat, Singel 425, 1012 WP Amsterdam, The Netherlands. You will be contacted as soon as possible.

UvA-DARE is a service provided by the library of the University of Amsterdam (<https://dare.uva.nl>)

Mechanistic Basis for Red Light Switching of Azonium Ions

Miroslav Medved,^{‡‡} Mariangela Di Donato,^{‡‡} Wybren Jan Buma, Adèle D. Laurent, Lucien Lameijer, Tomáš Hrivnák, Ivan Romanov, Susannah Tran, Ben L. Feringa, Wiktor Szymanski,* and G. Andrew Woolley*



Cite This: *J. Am. Chem. Soc.* 2023, 145, 19894–19902



Read Online

ACCESS |



Metrics & More

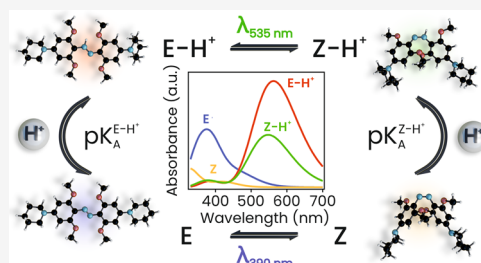


Article Recommendations



Supporting Information

ABSTRACT: Azonium ions formed by the protonation of tetra-*ortho*-methoxy-substituted aminoazobenzenes photoisomerize with red light under physiological conditions. This property makes them attractive as molecular tools for the photocontrol of physiological processes, for example, in photopharmacology. However, a mechanistic understanding of the photoisomerization process and subsequent thermal relaxation is necessary for the rational application of these compounds as well as for guiding the design of derivatives with improved properties. Using a combination of sub-ps/ns transient absorption measurements and quantum chemical calculations, we show that the absorption of a photon by the protonated *E*-H⁺ form of the photoswitch causes rapid (ps) isomerization to the protonated *Z*-H⁺ form, which can also absorb red light. Proton transfer to solvent then occurs on a microsecond time scale, leading to an equilibrium between *Z* and *Z*-H⁺ species, the position of which depends on the solution pH. Whereas thermal isomerization of the neutral *Z* form to the neutral *E* form is slow ($\sim 0.001\text{ s}^{-1}$), thermal isomerization of *Z*-H⁺ to *E*-H⁺ is rapid ($\sim 100\text{ s}^{-1}$), so the solution pH also governs the rate at which *E*/*E*-H⁺ concentrations are restored after a light pulse. This analysis provides the first complete mechanistic picture that explains the observed intricate photoswitching behavior of azonium ions at a range of pH values. It further suggests features of azonium ions that could be targeted for improvement to enhance the applicability of these compounds for the photocontrol of biomolecules.



1. INTRODUCTION

Molecular photoswitches¹ have diverse applications ranging from control of catalysis² to control of material properties³ and control of biological targets.^{4–8} For each of these applications, the wavelength of light used for photoswitching can be important. For biomedical applications, photoswitches that operate in the red/near-IR region of the visible spectrum are of particular interest.^{9–14} Red light is highly penetrating in biological tissues and has minimal adverse effects.¹⁵ However, very few molecular photoswitches can be reliably isomerized in aqueous conditions with red light in a reversible manner without degradation.^{14,16–26} A notable exception is the azonium ion formed by protonation of tetra-*ortho*-methoxy-substituted di-aminoazobenzene. Typically, azonium ions are formed at low pH (<pH 3), and their thermal *Z*-H⁺-to-*E*-H⁺ isomerization occurs on the microsecond time scale.²⁷ Both these features are unsuitable for biological applications where substantial light-induced production of the *Z* or *Z*-H⁺ form of the photoswitch at neutral pH is desired (e.g., typical cytoplasmic pH is 7.3).²⁸ Azonium ions formed by tetra-*ortho*-methoxy-substituted aminoazobenzenes are distinct in this respect since they form at pH 7, photoisomerize with red light, and thermally relax on the time scale of seconds.^{11,29,30} These properties enable photopharmacology applications such as *in vivo* enzyme inhibition and targeting receptor signaling.³¹ The unexpected properties of tetra-*ortho*-methoxy-substituted

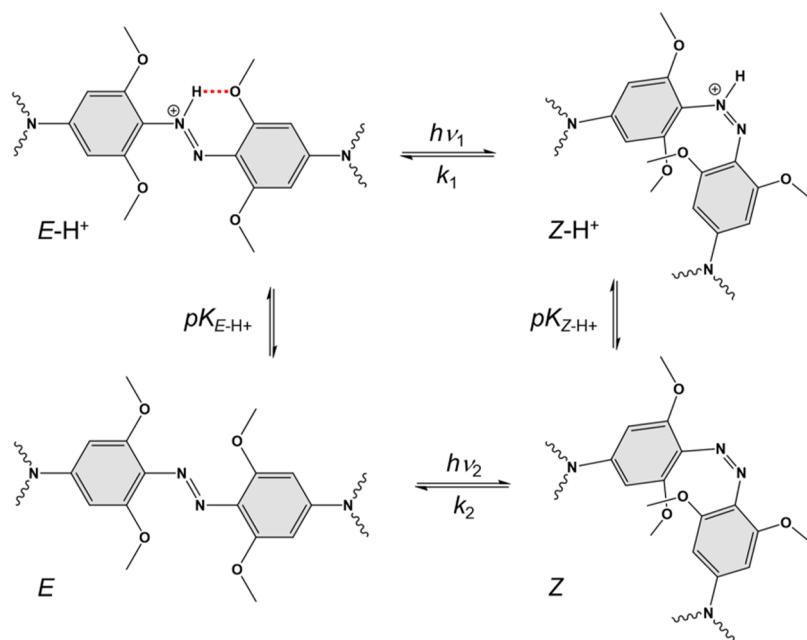
aminoazobenzenes increase a number of mechanistic questions. In previous work, it was suggested that the *E*-H⁺ azonium ion was stabilized by the presence of multiple electron-donating groups as well as by hydrogen bonding to the *ortho* methoxy oxygen substituent, increasing the azonium pK_a .²⁹ Photoisomerization to the *Z*-H⁺ azonium ion was proposed to occur, altering the geometry so that the intramolecular H-bond formation is less favorable (Scheme 1), and the pK_a is lower. In appropriate pH ranges, photoisomerization to *Z*-H⁺ then leads to deprotonation to the *Z* form, for which thermal relaxation is slower as compared to the protonated form.

However, in principle, other processes might occur after the absorption of a photon, including proton dissociation from the excited state or excited-state intramolecular proton transfer (ESIPT) from the azonium nitrogen to a methoxy oxygen. Understanding the details of how this photoswitch operates is critical for optimization of the design including improving the

Received: June 12, 2023

Published: September 1, 2023



Scheme 1. Photoisomerization and Acid–Base Equilibria of Tetra-*ortho*-methoxy-substituted Aminoazobenzenes^a

^aThe intramolecular H-bond stabilizing the $E-H^+$ azonium ion is drawn in red.

wavelength of isomerization, the degree of photoswitching, the rate of thermal relaxation, and the relative stability of the neutral and protonated E and Z isomeric forms. Here, we take a multifaceted approach using transient absorption spectroscopy and computational methods to deduce the detailed mechanism of photoisomerization of a representative example of this important class of compounds.

2. RESULTS AND DISCUSSION

2.1. Synthesis, Conformations, and Spectra of E -Isomers. Compound **1**, (E)-1,2-bis(2,6-dimethoxy-4-(piperidin-1-yl)phenyl)diazene (Figure 1), was synthesized using methods developed previously (see Section S1).²⁹ The piperidine substituent in the *para*-positions of the compound was chosen based on previous studies on the effect of different amino group donors on the azonium pK_a .¹¹ The thermal relaxation rate of this compound at neutral pH is < 1 s (*vide infra*), somewhat shorter than previously reported for other tetra-*ortho*-methoxy-substituted aminoazobenzenes.³²

The UV–vis electronic absorption spectrum of dark-adapted **1** was obtained in aqueous buffer as a function of pH (Figures 1a and S3.1). At high pH values (>9), the pale, yellow-colored neutral species (E) predominates. The purple-colored singly protonated azonium ion ($E-H^+$) predominates at physiological pH (7.0). At lower pH values, the yellow-colored doubly protonated species ($E-2H^{2+}$) is formed. The fitting of absorbance data gives a pK_a for the $E-H^+$ species of 7.7 and a pK_a for $E-2H^{2+}$ species of 4.2 (Figure 1b).

Relative stabilities of ground-state structures of **1** in different protonation states were calculated at the density functional theory (DFT) level using the M06-2X functional³³ in combination with the 6-31+G(d) atomic basis set³⁴ (Table S8.1). A $pK_a = 6.8$ for $E-H^+$ was estimated using the protocol proposed by Lian et al.³⁵ (Table S9.1). This value is ~ 1 pH unit lower than the value calculated from the titration data (7.7; Figure 1b). The $E-H^+$ species is calculated to be ~ 4 kcal/mol lower in energy than $Z-H^+$ (Table S8.1). Gibbs

energies indicate that the neutral E species is ~ 2 kcal/mol more stable than the Z isomer (Table S8.1), and NMR data in methanol (Figure S4.2) confirm that, at equilibrium in the dark, the fraction of Z species (Z and $Z-H^+$) is less than $\sim 3\%$.

The origins of spectral transitions were examined using a composite approach combining the second-order approximate coupled-cluster (CC2) method³⁶ with time-dependent density functional theory (TD-DFT) employing the CAM-B3LYP functional³⁷ and the universal solvation model based on solute electron density (SMD)³⁸ to account for the solvent effects within the linear-response (LR) and corrected LR (cLR) formalisms^{39,40} (see computational details in Section S7).

In the case of the neutral E form, both planar and distorted conformers with similar thermodynamic stability in aqueous solution were identified. These are separated by a very small (~ 1 kcal/mol) barrier so that a large region on the potential energy surface (PES) of E is relatively flat, and the molecules can adopt various conformations. Calculations indicate that planar conformers exhibit a single relatively intense peak at ~ 400 nm corresponding to the $S_0 \rightarrow S_2$ transition (the S_1 state is dark), while distorted structures show two bands (the $S_0 \rightarrow S_1$ transition gains some intensity) giving rise to a long-wavelength tail in the spectrum. This behavior is also seen in QM/MM/PE molecular dynamics simulations (Section S11). The experimentally observed two-band structure of the absorption spectra of the neutral E form in solution (Figure 1a) is therefore attributed to the coexistence of planar and distorted conformers in solution.

CC2//TD-DFT calculations indicate that the intense, red-shifted absorption ($\lambda_{\max} \sim 540$ nm) of the $E-H^+$ form is associated with a quasi-planar $E-H^+$ structure and is due to an $S_0 \rightarrow S_1$ ($\pi\pi^*$) transition that exhibits charge-transfer character (Figure 1c) (see the Supporting Information, Section S10.d). Further protonation to produce $E-2H^{2+}$ preserves the $\pi\pi^*$ character of the bright $S_0 \rightarrow S_1$ transition, but less π -electron delocalization (disrupted by the second protonation) results in a blue shift of the absorption maximum ($\lambda_{\max} \sim 480$ nm).

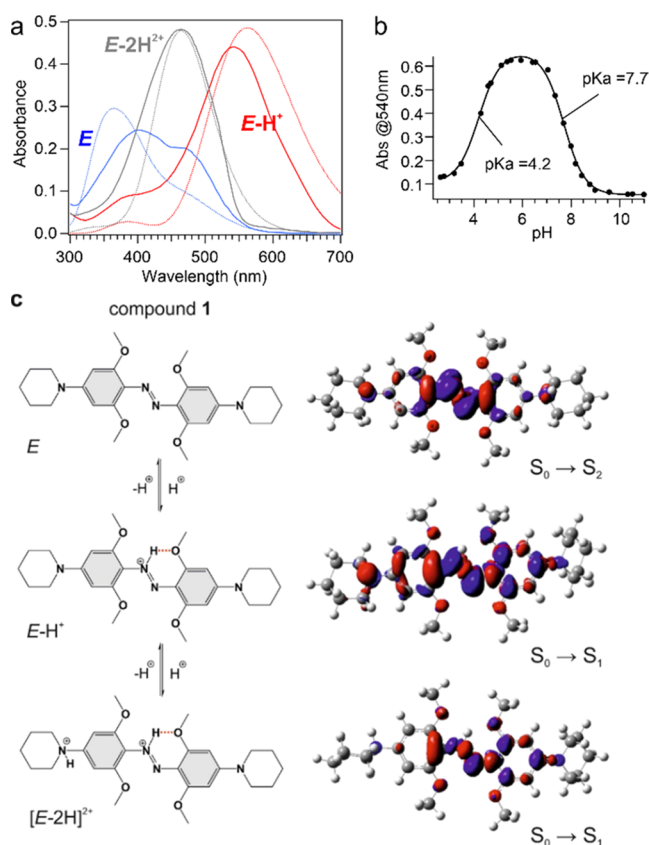


Figure 1. (a) Experimental and theoretical UV–vis electronic absorption spectra of compound 1. Experimental spectra (solid lines) were derived from titration curves using singular value decomposition (SVD) analysis. Simulated spectra (FWHM = 0.8 eV) were obtained using the composite CC2//LR-cLR-CAM-B3LYP/SMD approach (see computational details in the SI). (b) Analysis of absorbance at 540 nm vs. pH can be fitted to obtain pK_a 's of 7.7 and 4.2 for the singly and doubly protonated E species, respectively. (c) Acid–base equilibria between E -isomers in neutral, singly, and doubly protonated forms and the corresponding electron density difference (EDD) plots for the optimized structures showing the decrease (red) and increase (blue) of the electron density upon the indicated transitions (isovalue = 0.0015 au).

Since we are interested particularly in applications near neutral pH, we focused here on studying the behavior of the neutral and singly protonated forms of the compound.

2.2. Electronic Excitation of $E-H^+$. Absorption of a photon of 535 nm wavelength by $E-H^+$ produces an excited state ($E-H^+$)*. In this state, proton transfer to solvent (ESPT) or ESIPT from the azonium nitrogen to the oxygen of the methoxy group may occur (Scheme S12.1). However, TD-DFT calculations show that the N–H bond in the optimized S_1 -state structure is shorter by ~ 0.01 Å than in the ground-state structure because of increased electron density along the bond upon excitation (see a blue lobe along the N–H bond in the EDD plot for the $S_0 \rightarrow S_1$ transition displayed in Figures 1c and S10.3). Consequently, $E-H^+$ would be expected to be a weaker acid in the excited state making proton transfer to solvent improbable. Despite a slight increase of the electron density on the methoxy oxygen, ESIPT was also found to be energetically unfavorable (Figure S12.2). Calculations also show a decrease in electron density along the N=N bond, bringing about its elongation by ~ 0.06 Å upon excitation (Figure S12.1). Weakening of the N=N bond suggests that

$E-H^{+*}$ may decay through a conical intersection either to $E-H^+$ or to $Z-H^+$. A minimum energy conical intersection structure was optimized using the spin-flip formulation of TD-DFT implemented in the Gamess program^{43,44} and features a pyramidal ammonium nitrogen (Figure S15.1, N3) and a torsion angle around the N=N bond of 112.5° (Figure S15.1). The latter is larger than the torsion angle found in the transition state for the thermal $Z-H^+/E-H^+$ rotation (97.5°) (Figure S8.4), suggesting a preference for nonradiative decay to $E-H^+$ over $Z-H^+$.

2.3. Transient Absorption Measurements. A solution of 1 in aqueous buffer (pH 6.85) was examined using both sub-picosecond and nanosecond transient absorption spectroscopies (see Section S5, S6 for experimental details). At this pH, the dark-adapted solution contains $\sim 90\%$ of the $E-H^+$ form and $\sim 10\%$ of the neutral E form. While the singly protonated azonium ion ($E-H^+$) photoswitches with red light, its peak absorbance is ~ 540 nm, which is why green light [530 nm (ps data), 535 nm (ns data)] was used to produce isomerization in the present work. This excitation wavelength is expected to be absorbed primarily by not only the $E-H^+$ species but also the E species, which has an absorption tail that extends to this wavelength (Figure 1) due to the presence of different conformations (quasi-planar and distorted).

The electronic absorption difference spectra obtained upon excitation with a 150 fs pulse centered at 530 nm are shown in Figure 2a (left panel). Spectral components (EADS, evolution-associated difference spectra) were extracted from these data using global analysis with a sequential three-component model (Figure 2a, right panel). Immediately after excitation, an intense negative signal with a peak at about 535 nm was observed, which we assign to ground-state bleaching. A less intense excited-state absorption (ESA) band was observed on the blue side, peaked at 440 nm and on the red side at 600 nm. The ground-state bleaching signal almost completely recovered on a fast (0.8 ps) time scale (evolution from the black to the red component in Figure 2a, right panel). On the same time scale, the 440 nm ESA signal also recovered, indicating that the sample reached the conical intersection region for isomerization, decaying on the ground-state potential energy surface. The substantial recovery of the ground-state bleaching signal may be explained if the absorption spectrum of $Z-H^+$ is similar to that of $E-H^+$, so that the production of $Z-H^+$ tends to cancel the $E-H^+$ bleaching signal. We discuss the characteristics of the absorbance spectrum of the $Z-H^+$ species in further detail below. Since the solution also contains $\sim 10\%$ of neutral E isomer, E -to- Z isomerization is also induced upon light absorption. Spectral signatures of this process are not observed since the bleaching of the E species, expected to peak at about 390 nm, is compensated for by the ESA band of $E-H^{+*}$. The second spectral component extracted from global analysis also showed a broad positive absorption band in the 550–700 nm range. We assign this to hot ground-state absorption of both $E-H^+$ and $Z-H^+$ isomers. This band completely recovered on a 5.4 ps time scale (evolution from the red to the blue component in Figure 2a, right panel) because of vibrational cooling. The final spectral component (blue line) is almost flat, implying spectral compensation between the absorption of the $E-H^+$ reactant and the $Z-H^+$ photoproduct. This spectral component lives well beyond the time scale accessed by the picosecond measurement.

Transient absorption measurements on a longer time scale were then performed on the same solution to investigate

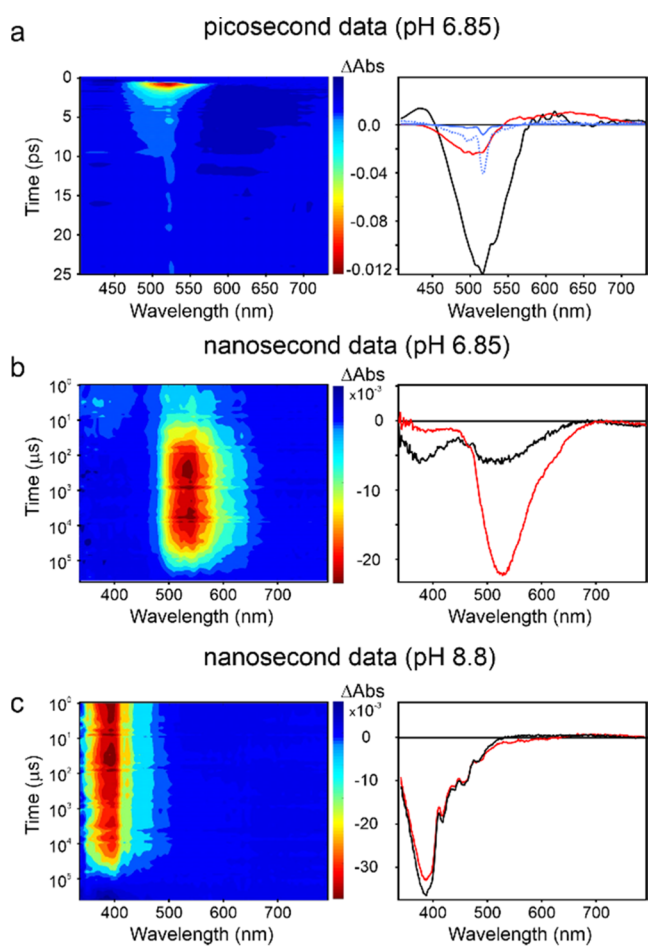


Figure 2. Transient absorption data for the electronic excitation of $E-H^+$. (a) Transient absorption data obtained upon sub-ps laser excitation at 530 nm of an aqueous sample solution at pH 6.85 at 20 ± 0.5 °C. EADS resulting from global analysis yields three components with lifetimes of 0.8 ps (black line), 5.4 ps (red line), and >1 ns (blue line; 5x expanded blue dotted line); (b) transient absorption data obtained upon ns laser excitation at 535 nm of a sample solution at pH 6.85 at 20 ± 0.5 °C. EADS resulting from global analysis yields two components with lifetimes of 42 μ s (black line) and 129 ms (red line). (c) Transient absorption data obtained upon ns laser excitation at 535 nm of a sample solution at pH 8.8. EADS resulting from global analysis yields two components with lifetimes of 199 μ s (black line) and 256 ms (red line).

processes occurring in the ground state after the production of $Z-H^+$ from $E-H^+$ (and Z from E) (Figure 2b). Upon excitation with an ns pulse centered at 535 nm, a weak negative signal was seen soon after light absorption, and subsequently a strong negative signal grew in on the μ s time scale. Observation of the growth of a negative signal over time is unusual; most time-resolved absorption difference data show rapid ground-state bleaching, which decays, rather than grows, with time.⁴⁵ We first analyzed the ns time-resolved data using a sequential two-component model. While this model is not expected to accurately represent all of the processes occurring after the pulse, it is useful for extracting the dominant spectral components and their lifetimes. The initial spectral component (black line in Figure 2b, right panel) has two negative bands peaking at ~ 390 and 540 nm. The strong negative band at 540 nm (red line) develops on a time scale of about 40 μ s and subsequently decays with a lifetime of 129 ms.

At higher pH (8.8), the solution contains about 90% E and 10% $E-H^+$. Nanosecond transient absorbance (TA) data again show two components (black and red lines); however, in this case, a strong negative signal was seen at 390 nm and the signal near 540 nm was almost zero. The lifetime of the first component was ~ 200 μ s and that of the second component was ~ 250 ms. Data were also acquired at a series of intermediate pH values, and EADS spectra intermediate between those shown in Figure 2b,c were obtained (Figure S6.1–2). In each case, two dominant lifetimes could be fitted to the data with one component on the μ s time scale (40–200 μ s) and a second component on the ms time scale (129–256 ms). As the pH increased, both lifetimes became longer (Table S6.1). We note that, for data obtained above \sim pH 7.3, the relaxation of the slow component was incomplete during the waiting time between ns pulses, so that quantitative analysis of these data is restricted to pH $<$ 7.3.

2.4. Mechanistic Analysis. To aid the interpretation of data obtained by transient absorption measurements, a detailed theoretical analysis of the photoactivated and thermal steps and the acid–base equilibria was performed. Figure 3 shows a

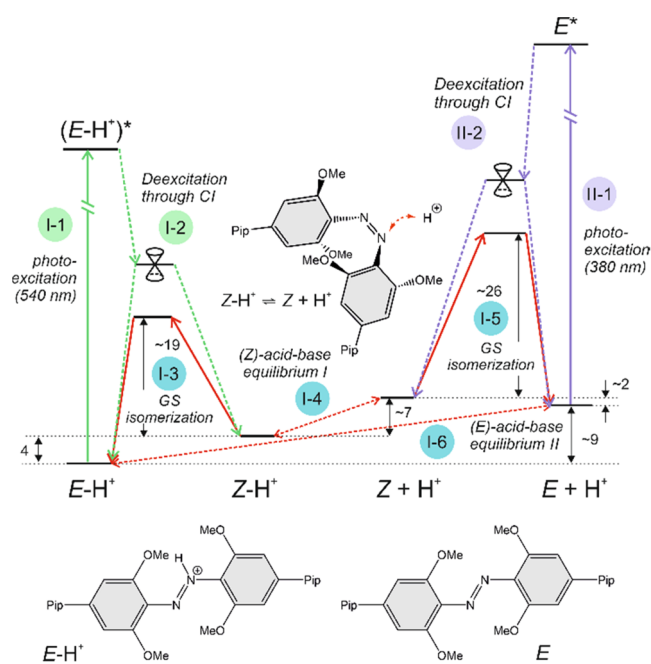


Figure 3. State diagram showing E , Z , $E-H^+$, and $Z-H^+$ ground-state species as well as excited states $(E-H^+)^*$ and $(E)^*$ formed by the absorption of a photon by $E-H^+$ and E of compound **1**, respectively. Energies (in kcal/mol) were obtained at the M06-2X/6-31+G(d) level of theory.

state diagram involving all relevant processes. The ground-state energetics and UV–vis absorption spectra of all species were calculated using the (TD-)DFT methodology supported by the domain-based local pair natural orbital coupled-cluster (DLPNO-CCSD(T))^{46–48} and CC2 methods, respectively (see computational details in Section S7).

The theoretical work suggests that $Z-H^+$ will absorb light of wavelengths almost the same as for $E-H^+$ but with a smaller ($\sim 50\%$) oscillator strength. Likewise, Z absorbs at similar wavelengths to E but with a significantly reduced absorption cross section. Thus, an initial weak bleach at 540 and 390 nm in the ns transient absorption spectra is consistent with the

photochemical conversion of $E-H^+$ to $Z-H^+$ and E to Z , occurring on a fast (ps) time scale. The absence of a 390 nm bleach in the ultrafast data is likely due to compensation by the ESA band peaking at 440 nm (Figure 2a).

After photochemical conversion of $E-H^+$ to $Z-H^+$ and E to Z , the system relaxes to the dark-state equilibrium. A kinetic scheme showing these ground-state processes is depicted in Figure 4a. We assumed that protonation/deprotonation

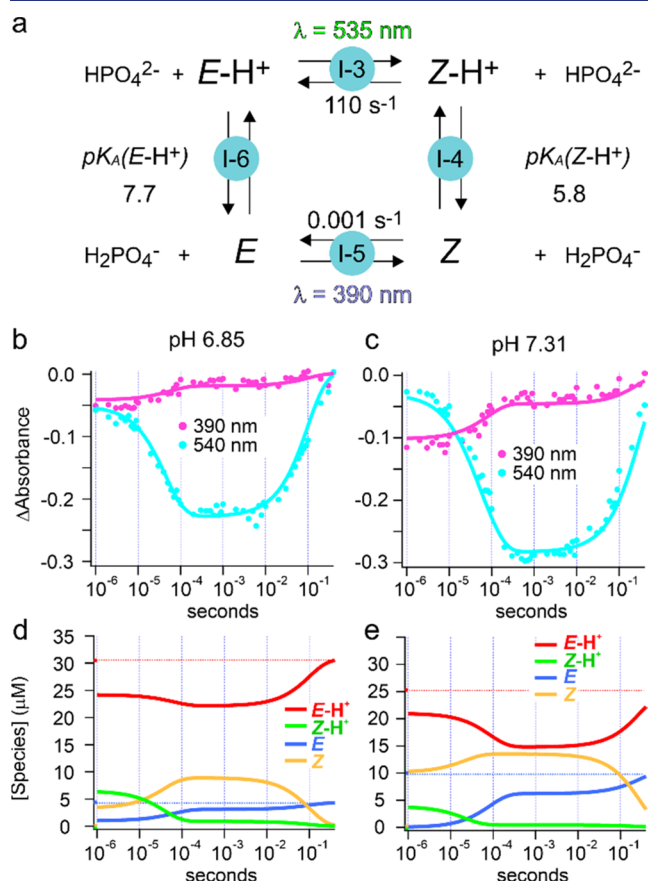


Figure 4. (a) Equilibria between species $E-H^+$, $Z-H^+$, E , and Z in the ground state. Light absorption converts E and $E-H^+$ to Z and $Z-H^+$. (b, c) Time-resolved absorbance difference measured at 390 nm (magenta) and 540 nm (cyan) after a nanosecond pulse for the system at pH 6.85 (b) and pH 7.31 (c) at 20 ± 0.5 °C. Fits calculated using Kintek Explorer are shown as solid lines. (d, e) Calculated concentrations of $E-H^+$, $Z-H^+$, E , and Z over time after a nanosecond pulse at pH 6.85 (d) and pH 7.31 (e), assuming the total concentration of **1** being $40 \mu\text{M}$.

reactions will be catalyzed by the phosphate buffer present^{49,50} and, for species with pK_a 's of 5–8, will occur in the microsecond time regime.⁵¹ This time scale is similar to the faster component observed in the ns transient absorbance measurements (Figure 2b).

We expect that the process occurring on the time frame of 125–250 ms (Figure 2b) reflects thermal back-isomerization of $Z-H^+$ to $E-H^+$. Thermal $Z-H^+$ -to- $E-H^+$ isomerization can, in principle, proceed either via rotation around the $N=N$ bond or via an N-inversion pathway. DFT calculations using relaxed scans followed by transition-state optimizations showed that the N-inversion pathway has a higher barrier (by ~ 6 kcal/mol; Table S8.1). The rotational barrier was calculated to be ~ 19 kcal/mol (Figure 3, I-3, and Table S8.1),

implying a relaxation time of seconds. However, the DFT approach applied here has been found to overestimate this barrier for azobenzenes by ~ 5 kcal/mol in polar solvents⁵² so that thermal isomerization on a 125–250 ms time scale is plausible.

In principle, the neutral Z species may also isomerize to E , but the barrier for the rotational pathway for this process was calculated to be ~ 26 kcal/mol (Figure 3, I-5, and Table S8.1), substantially higher than for the protonated species. The inversion pathway was found to be even more energetically demanding (~ 32 kcal/mol, Table S8.1). The rate constant for thermal isomerization of Z to E at pH 11.6 was measured experimentally to be 0.001 s^{-1} (Figure S4.1).

In addition to these estimates of rate constants, the pK_a of $E-H^+$ is known (Figure 1) as well as the spectra of $E-H^+$ and E species. Using these constraints, we performed global fitting of the time-resolved absorption difference data as a function of pH to the model in Figure 4a using Kintek Explorer software.⁵³ Fitted parameters include the rate constant for isomerization of $Z-H^+$ to $E-H^+$, the pK_a of $Z-H^+$, the fraction of $E-H^+$ and E isomerized by the pulse, and molar extinction coefficients for $Z-H^+$ and Z . An estimate of the molar extinction coefficient of Z was also made by applying the method of Fischer⁵⁴ to photoswitching data in methanol (Figure S4.3). Further details of the global fitting process are given in the SI (Section S16).

Figure 4b shows time-resolved kinetic traces measured at 390 nm and 540 nm during dark relaxation of the sample at pH 6.85. Fits to the data are shown as solid lines. Figure 4d shows species concentrations over time as determined by global fitting; the dark-adapted equilibrium concentrations are shown with dotted lines. At this pH, the $E-H^+$ species dominates at equilibrium (90%). The light pulse produces $Z-H^+$ from $E-H^+$ and then $Z-H^+$ loses a proton to form Z . The rate constant for proton dissociation from $Z-H^+$ (to HPO_4^{2-}) determines the fast time constant ($40 \mu\text{s}$) observed at this pH. Eventually, $E-H^+$ is restored via the thermal isomerization of $Z-H^+$, which is in equilibrium with Z and the position of this equilibrium is dictated by the solution pH (Figure 4a, I-3, I-4). The time constant for this process depends on the rate constant for thermal isomerization and on the pH. Higher pH values make the protonation of Z less likely. At pH 6.85, a time constant of 129 ms was observed.

Figure 4c shows time-resolved kinetic traces, and Figure 4e shows species concentrations during the dark relaxation of the sample measured at pH 7.31. At this pH, there is a substantial fraction of E at equilibrium ($\sim 30\%$). As before, $E-H^+$ is switched to $Z-H^+$ and loses a proton. In addition, a substantial fraction of Z is produced directly from photoisomerization of E . Even though the wavelength of the 535 nm nanosecond pulse is absorbed more efficiently by $E-H^+$ than by E , E -to- Z isomerization appears more efficient than $E-H^+$ -to- $Z-H^+$ isomerization, perhaps because of the hydrogen bond that stabilizes the $E-H^+$ species or because E can adopt twisted geometries that facilitate isomerization. As a result, after the pulse, the $E-H^+/E$ equilibrium is restored by the loss of a proton from $E-H^+$ to form E . The process also contributes to the absorbance changes seen in the microsecond time regime. Since the rate constant for the dissociation of $E-H^+$ is smaller than for dissociation of $Z-H^+$ (as expected, since $E-H^+$ is a weaker acid⁵⁵), the time constant observed at pH 7.31 ($77 \mu\text{s}$) is longer than at pH 6.85 ($40 \mu\text{s}$). Restoration of $E-H^+$ is also slower (202 ms at pH 7.31 vs. 129 ms at pH 6.85) (cf. Figure

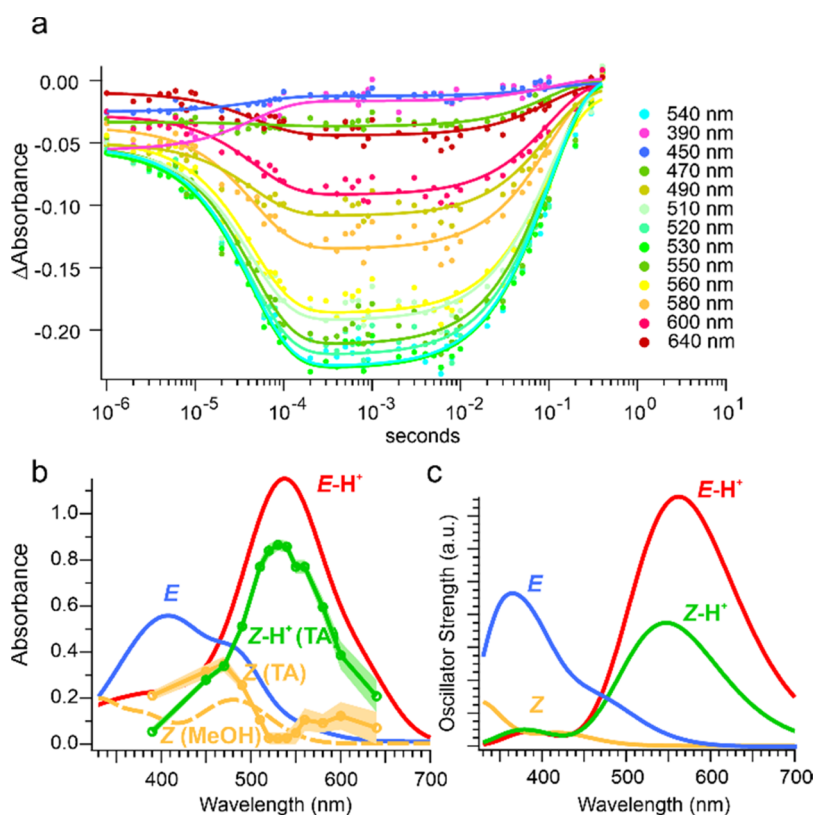


Figure 5. (a) Time-resolved absorbance difference measured at the wavelengths indicated after a nanosecond pulse for the system at pH 6.85 at 20 ± 0.5 °C. (b) Calculated spectra using the fits to transient absorbance (TA) data in panel (a) for $Z-H^+$ and Z . The spectrum of Z in methanol calculated as described in the SI is shown in dashed lines. Spectra of $E-H^+$ and E (see Figure 1) are shown for reference. (c) Theoretical UV-vis spectra of E , Z , $E-H^+$, and $Z-H^+$ species obtained by a composite CC2/def2-TZVPP//CAM-B3LYP/6-31++G(2df,2p)/SMD/LR+cLR approach (see Section S10 in the SI).

4e vs. 4d) because the protonation of Z to form $Z-H^+$ is less likely at higher pH.

Global fitting was performed for the nanosecond transient absorbance data over the pH range of 5.9–7.31. Fits to other pH values (pH 5.9, pH 7.02, pH 7.12, pH 7.21) are shown in Figure S16.1. A thermal isomerization rate constant for $Z-H^+$ -to- $E-H^+$ isomerization of 110 s^{-1} and a pK_a of $Z-H^+$ of 5.84 could be used to fit all of the data. The rate constant is consistent with a barrier height of 14–15 kcal/mol, somewhat lower than predicted (Figure 3, I-3). The pK_a obtained for $Z-H^+$ (5.84) is slightly higher than that predicted by calculation (pK_a 5.2); the methods employed also underestimate the pK_a obtained for $E-H^+$ by direct titration (6.8 vs. 7.7) (Table S9.1).

Kinetic traces as a function of wavelength provide information on the absorptivity of $Z-H^+$ and Z . Figure 5a shows these data for pH 6.85. Using the values of other parameters obtained from global fitting at all pH values, absorptivity values for $Z-H^+$ and Z were extracted. These are plotted to produce the spectral $Z-H^+$ and Z shown in Figure 5b along with spectra obtained for $E-H^+$ and E (Figure 1). The calculated spectra displayed in Figure 5c qualitatively reproduce the observed spectral features not only for the long-living $E-H^+$ and E -isomers (as discussed in Section 2.1) but also for the metastable $Z-H^+$ and Z species. The $Z-H^+$ isomer absorbs in the same region as $E-H^+$ ($\lambda_{\text{max}} = 547 \text{ nm}$), preserving the $\pi\pi^*$ character of the $S_0 \rightarrow S_1$ transition (Table S10.4 and Figure S10.4). However, the oscillator strength is smaller (ca. 50%) for $Z-H^+$. This decrease may be attributed

to the twisted geometry of $Z-H^+$, which leads to less electron delocalization. The spectral features of Z are much less pronounced compared to other species, which can be attributed to a mixed $n\pi^*/\pi\pi^*$ character of the $S_0 \rightarrow S_1$ transition (Table S10.6 and Figure S10.5). The predicted weak absorption band peaking at 420 nm is somewhat blue-shifted compared to that derived using the Fischer method and TA, but it should be noted that the VEE of this transition was found to be particularly sensitive to the applied method (Table S10.1).

2.5. Implications for the Use of Azonium Ions as Photoswitches. As described above, photoswitches that respond to red light and that operate under physiological conditions remain scarce despite being highly appealing as components for light-controlled tools in biomedicine, including photopharmacology tools.^{56,57} In a typical application of such a switch, the E isomer would be inactive, and the Z isomer would trigger a biological response (e.g., by blocking an ion channel or inhibiting an enzyme). If the response depends primarily on the geometry of the switch, both Z and $Z-H^+$ would be active and $E/E-H^+$ would be inactive. Effective photocontrol requires that the concentration of $Z/Z-H^+$ be negligible in the dark and that substantial conversion occurs upon irradiation with red light. This would be conveniently applied using a continuous LED source operating in the 10 mW/cm^2 range, but higher and lower powers and pulsed sources may also be used. Using the rate constants for the azonium switching process derived here (Figure 4a), one can predict the steady-state concentrations of species (e.g., Z and

$Z-H^+$) and how these would vary with light intensity and wavelength. If red light (e.g., 650 nm) is used, we may assume that both $E-H^+$ and $Z-H^+$ absorb and that E and Z do not absorb significantly. Starting from the dark equilibrium, a red beam produces $Z-H^+$ at a rate governed by the light intensity and the quantum yield for $E-H^+$ -to- $Z-H^+$ isomerization. The fraction of $Z/Z-H^+$ at steady state depends on how effectively this rate competes with the rate of thermal relaxation to reform $E-H^+$. As noted above, the quantum yield for $E-H^+$ -to- $Z-H^+$ photoisomerization appears significantly lower than that for E -to- Z photoisomerization. This is confirmed by steady-state measurements where larger changes in E/Z populations are seen upon irradiation at E wavelengths (e.g., 405 nm) vs. irradiation at $E-H^+$ wavelengths (595 nm) (Figure S4.1). In principle, a larger steady-state fraction of $Z/Z-H^+$ could be produced simply by increasing the light intensity. However, as light intensity is increased, the average time between absorption events decreases and can be estimated to be $<100 \mu\text{s}$ when light intensities exceed 100 W/cm^2 , as in microscopic imaging experiments.^{5,8} Depending on the solution pH, the lifetime of $Z-H^+$ is on the order of $100 \mu\text{s}$. Thus, if the light intensity is too high, $Z-H^+$ may absorb a 650 nm photon and be converted back to $E-H^+$ before it can dissociate to form Z . Modifications of the photoswitch structure that lowered the pK_a of $Z-H^+$ while maintaining the pK_a of $E-H^+$ (to maintain red light absorption at physiological pH) would result in faster deprotonation so that higher light intensities could be used. Lowering the pK_a of $Z-H^+$ would also slow thermal relaxation, which proceeds via $Z-H^+$. Chemical modifications that shift the wavelength of absorbance of $Z-H^+$ relative to $E-H^+$ would also enable higher light intensities to be used since they would reduce the possibility of photoconversion of $Z-H^+$ back to $E-H^+$. Finally, modifications that enhanced the quantum yield for $E-H^+$ -to- $Z-H^+$ photoisomerization would enhance the degree of photoconversion even at low light intensities. If this quantum yield is kept low by the presence of a H-bond in the $E-H^+$ species, increasing it may prove difficult. Further analysis of the factors influencing the $E-H^+$ -to- $Z-H^+$ photoisomerization quantum yield may suggest approaches for improving it.

3. CONCLUSIONS

We have developed a quantitative mechanistic description of photoswitching of tetra-*ortho*-methoxy azonium ions in aqueous solutions, representing the first detailed mechanistic insight into the photochemistry of a unique class of molecular photoswitches that can be operated with red/near-IR light in biological context, including whole blood. This description explains the observed photoswitching behavior at a range of pH values. It further suggests features of these azonium ions that could be targeted for improvement to enhance the applicability of these compounds as photoswitches that operate with red light under physiological conditions.

■ ASSOCIATED CONTENT

SI Supporting Information

The Supporting Information is available free of charge at <https://pubs.acs.org/doi/10.1021/jacs.3c06157>.

Supplemental methods and additional experimental data: synthesis, transient absorption spectroscopy and kinetic fitting, details of calculations including electronic transitions and consideration of explicit water molecules;

thermal isomerization barriers for protonated and neutral forms (PDF)

Calculated structure for $E-H^+$ (XYZ)

Calculated structure for $Z-H^+$ (XYZ)

Calculated structure for Z (XYZ)

Calculated structure for E (conformation A) (XYZ)

Calculated structure for E (conformation B) (XYZ)

Calculated structure for E (conformation C) (XYZ)

Calculated structure for E (conformation D) (XYZ)

Calculated structure for $E-2H^{2+}$ (XYZ)

Calculated structure for $E-H^+$ (S1 excited state) (XYZ)

Minimum energy conical intersection (MECI) for protonated species (XYZ)

Minimum energy conical intersection (MECI) for neutral species (XYZ)

Transition state for rotation $Z-H^+$ to $E-H^+$ (XYZ)

Transition state for rotation Z to E (XYZ)

Transition state for inversion $Z-H^+$ to $E-H^+$ (XYZ)

Transition state for inversion Z to E (XYZ)

■ AUTHOR INFORMATION

Corresponding Authors

Wiktor Szymanski – Stratingh Institute for Chemistry, University of Groningen, 9747AF Groningen, The Netherlands; Medical Imaging Center, University Medical Center Groningen, 9713GZ Groningen, The Netherlands; orcid.org/0000-0002-9754-9248; Email: w.szymanski@umcg.nl

G. Andrew Woolley – Department of Chemistry, University of Toronto, Toronto M5S 3H6, Canada; orcid.org/0000-0002-3446-2639; Email: andrew.woolley@utoronto.ca

Authors

Miroslav Medved' – Regional Centre of Advanced Technologies and Materials, Czech Advanced Technology and Research Institute (CATRIN), Palacký University, Olomouc 783 71, Czech Republic; Department of Chemistry, Faculty of Natural Sciences, Matej Bel University, 974 01 Banská Bystrica, Slovak Republic; orcid.org/0000-0001-8599-1031

Mariangela Di Donato – LENS, European Laboratory for Non-Linear Spectroscopy, 50019 Sesto Fiorentino, FI, Italy; CNR-ICCOM, 50019 Sesto Fiorentino, FI, Italy; orcid.org/0000-0002-6596-7031

Wybren Jan Buma – Van 't Hoff Institute for Molecular Sciences, University of Amsterdam, 1098 XH Amsterdam, The Netherlands; Institute for Molecules and Materials, FELIX Laboratory, Radboud University, 6525 ED Nijmegen, The Netherlands; orcid.org/0000-0002-1265-8016

Adèle D. Laurent – Nantes Université, CNRS, CEISAM, UMR 6230, F-44000 Nantes, France; orcid.org/0000-0001-9553-9014

Lucien Lameijer – Stratingh Institute for Chemistry, University of Groningen, 9747AF Groningen, The Netherlands; Medical Imaging Center, University Medical Center Groningen, 9713GZ Groningen, The Netherlands; orcid.org/0000-0003-2841-4742

Tomáš Hrivnák – Department of Chemistry, Faculty of Natural Sciences, Matej Bel University, 974 01 Banská Bystrica, Slovak Republic; Polymer Institute, Slovak Academy of Sciences, 845 41 Bratislava, Slovak Republic

Ivan Romanov – Van 't Hoff Institute for Molecular Sciences, University of Amsterdam, 1098 XH Amsterdam, The Netherlands

Susannah Tran – Department of Chemistry, University of Toronto, Toronto MSS 3H6, Canada

Ben L. Feringa – Stratingh Institute for Chemistry, University of Groningen, 9747AF Groningen, The Netherlands;
orcid.org/0000-0003-0588-8435

Complete contact information is available at:
<https://pubs.acs.org/10.1021/jacs.3c06157>

Author Contributions

††M.M. and M.D.D. contributed equally to this work. The manuscript was written through contributions of all authors. All authors have given approval to the final version of the manuscript.

Funding

This work was supported by the Slovak Research and Development Agency (APVV-20-0098 to M.M.), the Ministry of Education, Youth and Sports of the Czech Republic through the e-INFRA CZ (ID: 90254) and the COST Action CA21101 (to M.M.), the European Union's Horizon 2020 research and innovation program under grant agreement no. 871124 Laserlab-Europe (to M.D.D.), the Dutch Science Organization NWO ECHO Grant (711.017.012, to W.S.), the EUR LUMOMAT project and the Investments for the Future program ANR-18-EURE-0012, and the Natural Sciences and Engineering Research Council of Canada (RGPIN-174255, to G.A.W.).

Notes

The authors declare no competing financial interest.

ABBREVIATIONS

CC2	second-order approximate coupled-cluster method
CI	conical intersection
EADS	evolution-associated difference spectra
EDD	electron density difference
ESA	excited-state absorption
ESIPT	excited-state intramolecular proton transfer
GS	ground state
TD-DFT	time-dependent density functional theory

REFERENCES

- (1) Feringa, B. L.; Browne, W. R. *Molecular Switches*, 2nd ed.; Wiley-VCH, 2011; p 476.
- (2) Stoll, R. S.; Peters, M. V.; Kuhn, A.; Heiles, S.; Goddard, R.; Buhl, M.; Thiele, C. M.; Hecht, S. Photoswitchable catalysts: Correlating structure and conformational dynamics with reactivity by a combined experimental and computational approach. *J. Am. Chem. Soc.* **2009**, *131*, 357–367.
- (3) Abendroth, J. M.; Bushuyev, O. S.; Weiss, P. S.; Barrett, C. J. Controlling motion at the nanoscale: Rise of the molecular machines. *ACS Nano* **2015**, *9*, 7746–7768.
- (4) Borowiak, M.; Kullmer, F.; Gegenfurtner, F.; Peil, S.; Nasufovic, V.; Zahler, S.; Thorn-Seshold, O.; Trauner, D.; Arndt, H. D. Optical manipulation of F-actin with photoswitchable small molecules. *J. Am. Chem. Soc.* **2020**, *142*, 9240–9249.
- (5) Reynders, M.; Trauner, D. Optical control of targeted protein degradation. *Cell Chem. Biol.* **2021**, *28*, 969–986.
- (6) Kolarski, D.; Miller, S.; Oshima, T.; Nagai, Y.; Aoki, Y.; Kobauri, P.; Srivastava, A.; Sugiyama, A.; Amaike, K.; Sato, A.; Tama, F.; Szymanski, W.; Feringa, B. L.; Itami, K.; Hirota, T. Photopharmacological manipulation of mammalian CRY1 for regulation of the circadian clock. *J. Am. Chem. Soc.* **2021**, *143*, 2078–2087.

(7) Velema, W. A.; Szymanski, W.; Feringa, B. L. Photopharmacology: beyond proof of principle. *J. Am. Chem. Soc.* **2014**, *136*, 2178–2191.

(8) Beharry, A. A.; Woolley, G. A. Azobenzene photoswitches for biomolecules. *Chem. Soc. Rev.* **2011**, *40*, 4422–4437.

(9) Broichhagen, J.; Frank, J. A.; Johnston, N. R.; Mitchell, R. K.; Smid, K.; Marchetti, P.; Bugliani, M.; Rutter, G. A.; Trauner, D.; Hodson, D. J. A red-shifted photochromic sulfonyleurea for the remote control of pancreatic beta cell function. *Chem. Commun.* **2015**, *51*, 6018–6021.

(10) Dong, M.; Babalhavaeji, A.; Collins, C. V.; Jarrah, K.; Sadovski, O.; Dai, Q.; Woolley, G. A. Near-infrared photoswitching of azobenzenes under physiological conditions. *J. Am. Chem. Soc.* **2017**, *139*, 13483–13486.

(11) Dong, M.; Babalhavaeji, A.; Hansen, M. J.; Kalman, L.; Woolley, G. A. Red, far-red, and near infrared photoswitches based on azonium ions. *Chem. Commun.* **2015**, *51*, 12981–12984.

(12) Hansen, M. J.; Lerch, M. M.; Szymanski, W.; Feringa, B. L. Direct and versatile synthesis of red-shifted azobenzenes. *Angew. Chem., Int. Ed.* **2016**, *55*, 13514–13518.

(13) Konrad, D. B.; Savasci, G.; Allmendinger, L.; Trauner, D.; Ochsenfeld, C.; Ali, A. M. Computational design and synthesis of a deeply red-shifted and bistable azobenzene. *J. Am. Chem. Soc.* **2020**, *142*, 6538–6547.

(14) Lentès, P.; Stadler, E.; Rohricht, F.; Brahms, A.; Grobner, J.; Sonnichsen, F. D.; Gescheidt, G.; Herges, R. Nitrogen bridged diazocines: Photochromes switching within the near-infrared region with high quantum yields in organic solvents and in water. *J. Am. Chem. Soc.* **2019**, *141*, 13592–13600.

(15) Welleman, I. M.; Hoorens, M. W. H.; Feringa, B. L.; Boersma, H. H.; Szymanski, W. Photoresponsive molecular tools for emerging applications of light in medicine. *Chem. Sci.* **2020**, *11*, 11672–11691.

(16) Di Donato, M.; Lerch, M. M.; Lapini, A.; Laurent, A. D.; Iagatti, A.; Bussotti, L.; Ihrig, S. P.; Medved, M.; Jacquemin, D.; Szymanski, W.; Buma, W. J.; Foggi, P.; Feringa, B. L. Shedding light on the photoisomerization pathway of donor-acceptor Stenhouse adducts. *J. Am. Chem. Soc.* **2017**, *139*, 15596–15599.

(17) Mallo, N.; Foley, E. D.; Iranmanesh, H.; Kennedy, A. D. W.; Luis, E. T.; Ho, J.; Harper, J. B.; Beves, J. E. Structure-function relationships of donor-acceptor Stenhouse adduct photochromic switches. *Chem. Sci.* **2018**, *9*, 8242–8252.

(18) Yang, Y.; Hughes, R. P.; Aprahamian, I. Near-infrared light activated azo-BF₂ switches. *J. Am. Chem. Soc.* **2014**, *136*, 13190–13193.

(19) Hoorens, M. W. H.; Medved, M.; Laurent, A. D.; Di Donato, M.; Fanetti, S.; Slappendel, L.; Hilbers, M.; Feringa, B. L.; Jan Buma, W.; Szymanski, W. Iminothioindoxyl as a molecular photoswitch with 100 nm band separation in the visible range. *Nat. Commun.* **2019**, *10*, No. 2390.

(20) Wegener, M.; Hansen, M. J.; Driessen, A. J. M.; Szymanski, W.; Feringa, B. L. Photocontrol of Antibacterial Activity: Shifting from UV to Red Light Activation. *J. Am. Chem. Soc.* **2017**, *139*, 17979–17986.

(21) Berdnikova, D. V. Design, synthesis and investigation of water-soluble hemi-indigo photoswitches for bioapplications. *Beilstein J. Org. Chem.* **2019**, *15*, 2822–2829.

(22) Petermayer, C.; Thumser, S.; Kink, F.; Mayer, P.; Dube, H. Hemiindigo: Highly bistable photoswitching at the biooptical window. *J. Am. Chem. Soc.* **2017**, *139*, 15060–15067.

(23) Simke, J.; Bosking, T.; Ravoo, B. J. Photoswitching of ortho-aminated arylazopyrazoles with red light. *Org. Lett.* **2021**, *23*, 7635–7639.

(24) Thumser, S.; Kottner, L.; Hoffmann, N.; Mayer, P.; Dube, H. H. All-red-light photoswitching of indirubin controlled by supra-molecular interactions. *J. Am. Chem. Soc.* **2021**, *143*, 18251–18260.

(25) Wages, F.; Lentès, P.; Griebenow, T.; Herges, R.; Peifer, C.; Maser, E. Reduction of photoswitched, nitrogen bridged N-acetyl diazocines limits inhibition of 17βHSD3 activity in transfected

human embryonic kidney 293 cells. *Chem. Biol. Interact.* **2022**, *354*, No. 109822.

(26) Klaue, K.; Garmshausen, Y.; Hecht, S. Taking photochromism beyond visible: Direct one-photon NIR photoswitches operating in the biological window. *Angew. Chem., Int. Ed.* **2018**, *57*, 1414–1417.

(27) Sanchez, A. M.; Barra, M.; de Rossi, R. H. On the mechanism of the acid/base-catalyzed thermal cis-trans isomerization of methyl orange. *J. Org. Chem.* **1999**, *64*, 1604–1609.

(28) Llopis, J.; McCaffery, J. M.; Miyawaki, A.; Farquhar, M. G.; Tsien, R. Y. Measurement of cytosolic, mitochondrial, and Golgi pH in single living cells with green fluorescent proteins. *Proc. Natl. Acad. Sci. U.S.A.* **1998**, *95*, 6803–6808.

(29) Samanta, S.; Babalhavaei, A.; Dong, M. X.; Woolley, G. A. Photoswitching of ortho-substituted azonium ions by red light in whole blood. *Angew. Chem., Int. Ed.* **2013**, *52*, 14127–14130.

(30) Yasuike, N.; Blacklock, K. M.; Lu, H. X.; Jaikaran, A. S. I.; McDonald, S.; Uppalapati, M.; Khare, S. D.; Woolley, G. A. Photoswitchable affinity reagents: Computational design and efficient red-light switching. *ChemPhotoChem* **2019**, *3*, 431–440.

(31) Hoorens, M. W. H.; Szymanski, W. Reversible, spatial and temporal control over protein activity using light. *Trends Biochem. Sci.* **2018**, *43*, 567–575.

(32) Samanta, S.; Beharry, A. A.; Sadovski, O.; McCormick, T. M.; Babalhavaei, A.; Tropepe, V.; Woolley, G. A. Photoswitching azo compounds in vivo with red light. *J. Am. Chem. Soc.* **2013**, *135*, 9777–9784.

(33) Zhao, Y.; Truhlar, D. G. The M06 suite of density functionals for main group thermochemistry, thermochemical kinetics, non-covalent interactions, excited states, and transition elements: two new functionals and systematic testing of four M06-class functionals and 12 other functionals. *Theor. Chem. Acc.* **2008**, *120*, 215–241.

(34) Ditchfield, R.; Hehre, W. J.; Pople, J. A. Self-consistent molecular-orbital methods. 9. Extended Gaussian-type basis for molecular-orbital studies of organic molecules. *J. Chem. Phys.* **1971**, *54*, 724–728.

(35) Lian, P.; Johnston, R. C.; Parks, J. M.; Smith, J. C. Quantum chemical calculation of $pK(a)$ s of environmentally relevant functional groups: carboxylic acids, amines, and thiols in aqueous solution. *J. Phys. Chem. A* **2018**, *122*, 4366–4374.

(36) Christiansen, O.; Koch, H.; Jorgensen, P. The 2nd-Order Approximate Coupled-Cluster Singles and Doubles Model CC2. *Chem. Phys. Lett.* **1995**, *243*, 409–418.

(37) Yanai, T.; Tew, D. P.; Handy, N. C. A new hybrid exchange-correlation functional using the Coulomb-attenuating method (CAM-B3LYP). *Chem. Phys. Lett.* **2004**, *393*, 51–57.

(38) Marenich, A. V.; Cramer, C. J.; Truhlar, D. G. Universal solvation model based on solute electron density and on a continuum model of the solvent defined by the bulk dielectric constant and atomic surface tensions. *J. Phys. Chem. B* **2009**, *113*, 6378–6396.

(39) Caricato, M.; Mennucci, B.; Tomasi, J.; Ingrosso, F.; Cammi, R.; Corni, S.; Scalmani, G. Formation and relaxation of excited states in solution: A new time dependent polarizable continuum model based on time dependent density functional theory. *J. Chem. Phys.* **2006**, *124*, No. 124520.

(40) Guido, C. A.; Chrayteh, A.; Scalmani, G.; Mennucci, B.; Jacquemin, D. Simple protocol for capturing both linear-response and state-specific effects in excited-state calculations with continuum solvation models. *J. Chem. Theory Comput.* **2021**, *17*, 5155–5164.

(41) Shao, Y. H.; Head-Gordon, M.; Krylov, A. I. The spin-flip approach within time-dependent density functional theory: Theory and applications to diradicals. *J. Chem. Phys.* **2003**, *118*, 4807–4818.

(42) Casanova, D.; Krylov, A. I. Spin-flip methods in quantum chemistry. *Phys. Chem. Chem. Phys.* **2020**, *22*, 4326–4342.

(43) Gordon, M. S.; Schmidt, M. W. Advances in Electronic Structure Theory: GAMESS a Decade Later. In *Theory and Applications of Computational Chemistry: The First Forty Years*; Dykstra, C. E.; Frenking, G.; Kim, K. S.; Scuseria, G. E., Eds.; Elsevier: Amsterdam, 2005; pp 1167–1189.

(44) Schmidt, M. W.; Baldridge, K. K.; Boatz, J. A.; Elbert, S. T.; Gordon, M. S.; Jensen, J. H.; Koseki, S.; Matsunaga, N.; Nguyen, K. A.; Su, S. J.; Windus, T. L.; Dupuis, M.; Montgomery, J. A. General atomic and molecular electronic-structure system. *J. Comput. Chem.* **1993**, *14*, 1347–1363.

(45) Farr, E. P.; Quintana, J. C.; Reynoso, V.; Ruberry, J. D.; Shin, W. R.; Swartz, K. R. Introduction to time-resolved spectroscopy: Nanosecond transient absorption and time-resolved fluorescence of eosin B. *J. Chem. Educ.* **2018**, *95*, 864–871.

(46) Purvis, G. D.; Bartlett, R. J. A Full Coupled-Cluster Singles and Doubles Model-the Inclusion of Disconnected Triples. *J. Chem. Phys.* **1982**, *76*, 1910–1918.

(47) Raghavachari, K.; Trucks, G. W.; Pople, J. A.; Headgordon, M. A 5th-Order Perturbation Comparison of Electron Correlation Theories. *Chem. Phys. Lett.* **1989**, *157*, 479–483.

(48) Riplinger, C.; Pinski, P.; Becker, U.; Valeev, E. F.; Neese, F. Sparse maps-A systematic infrastructure for reduced-scaling electronic structure methods. II. Linear scaling domain based pair natural orbital coupled cluster theory. *J. Chem. Phys.* **2016**, *144*, No. 024109.

(49) Sudmeier, J. L.; Evelhoch, J. L.; Jonsson, N. B. H. Dependence of NMR lineshape analysis upon chemical rates and mechanisms—Implications for enzyme histidine titrations. *J. Magn. Reson.* **1980**, *40*, 377–390.

(50) Hass, M. A. S.; Hansen, D. F.; Christensen, H. E. M.; Led, J. J.; Kay, L. E. Characterization of conformational exchange of a histidine side chain: Protonation, rotamerization, and tautomerization of His61 in plastocyanin from *Anabaena variabilis*. *J. Am. Chem. Soc.* **2008**, *130*, 8460–8470.

(51) Wong, F. H. C.; Fradin, C. Simultaneous pH and temperature measurements using pyranine as a molecular probe. *J. Fluoresc.* **2011**, *21*, 299–312.

(52) Hegeđušová, L.; Kutel', R.; Medved', M.; Pašteka, L. F.; Cigán, M.; Budzák, Š Thermal isomerization of phenylazoindoles: Inversion or rotation? That is the question. *Int. J. Quantum Chem.* **2023**, No. e27120.

(53) Johnson, K. A.; Simpson, Z. B.; Blom, T. Global kinetic explorer: a new computer program for dynamic simulation and fitting of kinetic data. *Anal. Biochem.* **2009**, *387*, 20–29.

(54) Fischer, E. Calculation of photostationary states in systems $A \leftrightarrow B$ when only A is known. *J. Phys. Chem. A* **1967**, *71*, 3704–3706.

(55) Eigen, M. Proton Transfer Acid-Base Catalysis + Enzymatic Hydrolysis. I. Elementary Processes. *Angew. Chem., Int. Ed.* **1964**, *3*, 1–19.

(56) Kobauri, P.; Dekker, F. J.; Szymanski, W.; Feringa, B. L. Rational Design in Photopharmacology with Molecular Photoswitches. *Angew. Chem., Int. Ed.* **2023**, *62*, No. e202300681.

(57) Hüll, K.; Morstein, J.; Trauner, D. In Vivo Photopharmacology. *Chem. Rev.* **2018**, *118*, 10710–10747.

(58) Spring, K. R. Fluorescence Microscopy. In *Encyclopedia of Optical and Photonic Engineering*, 2nd ed.; Hoffman, C.; Driggers, R., Eds.; CRC Press: Boca Raton, 2016; Vol. 1, pp 755–762.